Genetic Evolution of the Reflector Edge Treatment of a Single Offset-Fed Compact Antenna Test Range for 5G New Radio Applications

M. Dirix [1]
[1] Antenna Systems Solutions
C/ Isabel Torres, 9.-1º
Santander, 39011, Cantabria, Spain,
mdirix@asysol.com

S.F. Gregson [2, 3]
[2] Next Phase Measurements
11521 Monarch St, Garden Grove,
CA, USA

R. R. Dubrovka [3]
[3] Queen Mary University of London
School of Electronic Engineering
and Computer Sciences
London, UK

***Abstract*—While the size of the parabolic reflector in general determines the usable area of the quiet zone of a compact antenna test range (CATR) inside which a pseudo plane-wave condition is produced, the reflector edge treatment also plays a significant role in terms of overall quality and electromagnetic field distribution & uniformity, and especially so at mm-wave frequencies. Using modern powerful digital computational simulation technology in combination with genetic optimization, the edge treatment can be evolved for a specific CATR application as part of the design process. This is crucial as it attempts to maximize the performance of a given solution while ensuring efficient use of the available space which correspondingly provides an economical implementation. This is particularly important in 5G production test applications where, in many instances, multiple systems are required to be collocated within a given host building and in which case, the savings become multiplicative. In this paper the novel design methodology is introduced for the genetic optimization (GO) of blended rolled edge single offset reflector CATRs. Several edge blends and treatments are considered with the genetically optimized design parameter. For each variation the quiet-zone performances are compared and contrasted.**

***Index Terms*—5G NR, mm-Wave, Genetic Algorithm, OTA, Blended Rolled Edge, CATR.**

I. Introduction

Small size single offset reflector compact antenna test ranges (CATR) are becoming a standard in the field of active antenna measurements for 5G applications [1]. While the overall size of the parabolic reflector, and other parameters such as focal distance, limits the extent of the region in which a pseudo plane wave is produced, its edge treatment plays a significant role as well in the overall spatial response found therein [2]. The blended rolled edge [3] treatment was conceived as a means for gradually distributing the edge diffracted waves from the range feed horn outside the quiet zone (QZ), all the while maintaining a continuous smooth surface preventing any further disturbances induced thereof. The initial formulations of the blended rolled edge treatment indicated an optimization of the rolled edge using a derivate to shape the reflector in a specific pre-defined outline shape, *e.g.* rectangular. However, it was not investigated whether this pre-defined shape provided optimal QZ performance. Furthermore, even though initial investigations showed a benefit of the blended rolled edge over the alternative, widely used, serrated edge treatment [4], the research did not take into account the increase in wall illumination at wider angles of incidence that result from this design [2]. However, in [5] it was shown that taking a different approach to the standard rectangular shape has certain benefits in the scattering resulting from the chamber walls. Using a genetic optimization within the design procedure of a CATR allows a broad parameter-sweep to be conducted during the optimization of the edge treatment that specifically focuses on the CATR QZ electromagnetic performance, and that can be tailored specifically to the given range parameters (*i.e.* facility layout). In [6] the benefits of such optimization were demonstrated for the case of the serrated edge treatment and will be expanded for the blended rolled edge treatment in this paper. The description of the blended rolled edge treatment is presented in Section II, after which a short summary of the genetic optimization approach and algorithm verification is covered in Section III with results being presented and discussed in Section IV. The paper concludes in Section V.

II. Blended Rolled Edge Treatment

As the genetic optimization (GO) depends fundamentally upon the mathematical form of the blended rolled edge (BRE) reflector, a brief discussion of the form of that function is now presented. The definition of the BRE treatment in a cylindrical coordinate system (ρ', φ', z') is defined in the centre of the reflector $(x'_0 = x_{\text{offset}}; y'_0 = y_{\text{offset}}; z'_0 = z_{\text{offset}})$, and is given by,

$$\left.\begin{aligned} x' &= \rho' \cos\varphi' \\ y' &= \rho' \sin\varphi' \\ z' &= z' \end{aligned}\right\}. \tag{1}$$

Let the base paraboloid of revolution of the reflector be defined in the cylindrical coordinate system as,

$$\rho'^2 + 2\rho'(x_{\text{offset}} \cos\varphi' + y_{\text{offset}} \sin\varphi') = 4Fz', \tag{2}$$

which for all practical purposes is bounded physically by $\left(0 \le \rho' \le \rho'_j(\varphi')\right)$ and $(0 \le \varphi' \le 2\pi)$, where $\rho'_j(\varphi')$, for the given case, this determines the boundary between the parabolic primitive, and blended rolled edge treatment in the cylindrical coordinate system. The blended rolled edge treatment can then be expressed as [3],

$$\rho'(\gamma,\varphi) = \left[\gamma\frac{x_m}{\gamma_m}x_{p2}(\varphi)\right]\big(1-b(\gamma)\big) + \big[(a_e\sin\gamma)x_{p2}(\varphi) + b_e(1-\cos\gamma)y_{p2}(\varphi)\big]b(\gamma) + \rho_j'(\varphi') \quad (3)$$

and,

$$z'(\gamma,\varphi) = \left[\left(\gamma\frac{x_m}{\gamma_m}x_{p2}(\varphi) + \rho_j''(\varphi)\right)^2 \Big/ {}_{4F}\right]\big(1-b(\gamma)\big) + \big[(a_e\sin\gamma)x_{p3}(\varphi) + b_e(1-\cos\gamma)y_{p3}(\varphi) + z_j''(\varphi')\big]b(\gamma) - (x_{\text{offset}}\cos\varphi' + y_{\text{offset}}\sin\varphi')^2 \Big/ {}_{4F}, \quad (4)$$

with $0 \le \gamma \le \gamma_m$, $b(\gamma)$ the blending function and,

$$\rho_j''(\varphi') = \rho_j'(\varphi') + (x_{\text{offset}}\cos\varphi' + y_{\text{offset}}\sin\varphi'), \quad (5)$$

$$z_j''(\varphi') = \left(\rho_j''(\varphi')\right)^2 \Big/ {}_{4F}, \quad (6)$$

$$x_{p2}(\varphi) = -y_{p3}(\varphi) = 2F \Big/ \left(\left(\rho_j''(\varphi')\right)^2 + 4F^2\right)^{\frac{1}{2}}, \quad (7)$$

$$y_{p2}(\varphi) = x_{p3}(\varphi) = \rho_j''(\varphi') \Big/ \left(\left(\rho_j''(\varphi')\right)^2 + 4F^2\right)^{\frac{1}{2}}, \quad (8)$$

and γ the roll variable with $0 \le \gamma \le \gamma_m$ for $\rho > \rho_j'(\varphi')$. Here, the blending function varies gradually between zero and unity; and is typically cosine or cosine-squared in form [7], although other choices can be used with each having different impacts on the overall dimension of the reflector, *cf.* [2]. It is noted here that in the presented formulation of the blended rolled edge above, as opposed to the formulations presented within the original referenced work [3], the rolled edge parameters x_m,γ_m,a_e and b_e are considered global variables, and are thus independent of roll angle φ'. It was found, as this work was based on the optimization of the QZ field distribution instead of the continuity of the reflector surface profile and its derivatives at the boundary of the parabola and the rolled edge itself, that the symmetry of the resulting QZ fields does not indicate any further particular need for this individual optimization. In section IV the QZ field distributions that have led to this conclusion are examined further. Finally, the boundary $\rho_j'(\varphi')$ between the parabolic portion and the blended rolled edge treatment is defined in the x', y'-plane by,

$$x_j' = \begin{cases} R_{\text{QZ},x} + r_e(1-\cos\varphi') & 0 \le \varphi' \le \varphi_1 \\ \left(R_{\text{QZ},y} + r_e\right)\cot\varphi' - r_e\cos\varphi' & \varphi_1 \le \varphi' \le \varphi_2 \\ -R_{\text{QZ},x} - r_e(1+\cos\varphi') & \varphi_2 \le \varphi' \le \varphi_3, \\ -\left(R_{\text{QZ},y} + r_e\right)\cot\varphi' - r_e\cos\varphi' & \varphi_3 \le \varphi' \le \varphi_4 \\ R_{\text{QZ},x} + r_e(1-\cos\varphi') & \varphi_4 \le \varphi' \le 2\pi \end{cases} \quad (9)$$

$$y_j' = \begin{cases} \left(R_{\text{QZ},x} + r_e\right)\tan\varphi' - r_e\sin\varphi' & 0 \le \varphi' \le \varphi_1 \\ R_{\text{QZ},y} + r_e(1-\cos\varphi') & \varphi_1 \le \varphi' \le \varphi_2 \\ -\left(R_{\text{QZ},x} + r_e\right)\tan\varphi' - r_e\sin\varphi' & \varphi_2 \le \varphi' \le \varphi_3, \\ R_{\text{QZ},y} - r_e(1+\cos\varphi') & \varphi_3 \le \varphi' \le \varphi_4 \\ \left(R_{\text{QZ},x} + r_e\right)\tan\varphi' - r_e\sin\varphi' & \varphi_4 \le \varphi' \le 2\pi \end{cases} \quad (10)$$

with,

$$\varphi_1 = \tan^{-1}\left(\frac{R_{\text{QZ},y}+r_e}{R_{\text{QZ},x}+r_e}\right), \quad (11)$$

$$\varphi_2 = \pi + \tan^{-1}\left(\frac{R_{\text{QZ},y}+r_e}{-R_{\text{QZ},x}-r_e}\right), \quad (12)$$

$$\varphi_3 = \pi + \tan^{-1}\left(\frac{-R_{\text{QZ},y}-r_e}{-R_{\text{QZ},x}-r_e}\right), \quad (13)$$

$$\varphi_4 = 2\pi + \tan^{-1}\left(\frac{-R_{\text{QZ},y}-r_e}{R_{\text{QZ},x}+r_e}\right), \quad (14)$$

and $R_{\text{QZ},x}, R_{\text{QZ},y}$ is the radius of the QZ in x and y direction. Section IV below illustrates how the driving parameters, specifically the boundary, r_e and roll parameters x_m, γ_m, a_e, and b_e within these expressions are used to control and determine the BRE reflector surface profile.

III. Quiet Zone Simulation

A. Overview of Efficient Simulation Algorithm

The field which illuminates the CATR reflector can be determined from the far-field antenna pattern function of the CATR feed by reintroducing the spherical phase and loss factors [8], [9]. The fields reflected by the, assumed perfect electrical conducting (PEC) surface can then be obtained from the physical optics condition [8], [9]. Many different computational electromagnetic (CEM) modelling techniques have been harnessed for the prediction of fields in the Fraunhofer- or Fresnel-regions, and a number of these are described in detail in, *e.g.* [8, 9, 10] with the current element (CE) method providing a desirable combination of high accuracy and numerical efficiency. The CE method replaces the radiated fields with an equivalent, infinitely thin, surface current sheet $\underline{J_s}$ which is used as an equivalent source to the original impressed fields. The surface current across the reflector can be obtained from the incident magnetic fields and the surface unit normal with this being termed the physical-optics (PO) approximation [8]. Then, the magnetic fields radiated by an infinitesimal electric CE can be obtained from the vector potential & the free-space Green's function using [8], [9], [2],

$$d\underline{H}(\underline{P}) = \frac{da}{4\pi}\underline{J_s} \times \nabla\psi, \quad (15)$$

The corresponding elemental-electric-fields can then be obtained, to an extremely good approximation, from the elemental magnetic fields using the plane-wave condition where the field point only need be in the far-field of the *elemental* source. This last assumption improves the computational efficiency when compared to a direct, evaluation of the electric field [8], [9]. This is a requirement that is easily satisfied when the separation is larger than a few wavelengths and the reflector is sampled at, say, a sixth of a wavelength, which is a widely used meshing criteria. A detailed examination and verification of the use of this for serrated edge CATR simulation can be found presented in the open literature [9], [2].

A powerful feature of this simulation methodology is that the field propagation itself is embarrassingly parallelable [6]. Although in practice there is some computational overhead associated with breaking the problem up and distributing it amongst an ensemble of individual processors, with more effort being required to aggregate the complete CATR QZ field once computed, this yields a circa *n*-fold increase in efficiency where *n* is the number of available CPU cores. Most modern digital computers comprise several individual cores, with 4 to 64 being

typical. This makes the field propagation computation finish in much less than a second for the case of typical mm-wave CATRs intended for 5GNR test applications such as that considered herein. Clearly then, such an approach enables the range designer to run optimizations comprising tens of thousands of simulations in a matter of only a few hours, and it is this huge efficiency and power that underpins the successful use of genetic optimization that is utilized within this study.

Thus, this attractive modelling approach was harnessed and adapted to the simulation of BRE CATRs in two ways. First, the feed illumination of the reflector was limited to include only the non-geometrical-shaded region, *i.e.* where $\underline{\hat{u}} \cdot \underline{\hat{n}} \geq 0$. Here, $\underline{\hat{n}}$ is the outward pointing reflector surface unit-normal, and $\underline{\hat{u}}$ is the unit-vector from the focal point, which is assumed to be coincident and synonymous with the feed's phase center, to the elemental portion of the reflector surface. Similarly, the integration of the current elements in Equation 15 is restricted such that only current elements for which $\underline{\hat{u}'} \cdot \underline{\hat{n}} \geq 0$ are included where $\underline{\hat{u}'}$ is the unit-vector from the current element to the field point. Although this appears at first inspection as being a relatively minor adaptation, it has a notable impact on the resulting CATR quiet-zone field distribution which motivated further examination. As was the case in [9], verification by means of a comparison with a proprietary full-wave three-dimensional CEM simulation tool was performed and can be found presented in the next section.

B. Validation of the PO algorithm with FEKO

The CEM modelling technique described above was used to compute QZ performance predictions for an offset, blended rolled edge CATR at frequency of 26 GHz. Note, this is a *different* CATR design to the one presented in Section IV below. Each simulation used a Gaussian feed pattern as this provided a good representation of the choked horn feed, and a consistent range geometry with only the field propagation methodology and reflector surface profile calculation changing between the respective models. As in [10], Altair's proprietary electromagnetic simulation tool FEKO [11] was used to provide independent predictions of the BRE CATR QZ.

There are a few possible approaches for creating a BRE CATR model in Altair's FEKO [11]. Perhaps the simplest of these is to use one of the interchange CAD standards, *e.g.*, STEP, to transfer a mechanical model of the system into the software and to simulate it as it is. The advantage of this is clear, the created model would be very close to the original. However, there is very limited flexibility thereafter in terms of possible changes of parameters, *e.g.* meshing *etc*. and gross oversampling due to the polar form of the formulation which would very probably require a new imported mechanical model file for *any* change in configuration, design, or setup. For this reason, a decision was taken to reconstruct the reflector surface model within FEKO. Here, one could create a section of paraboloid, known as a "defining rectangle", and then add to it a blended surface. However, as noted above, the surface is rather complicated; and cannot be constructed from standard Euclidian primitives. This provides two clear choices, either to use a set of points to create a surface, which is a rather common case in some CAD software and has the aforementioned limitations; or to create a set of defining curves and to loft them together. The second approach was adopted as it provided a soluble problem-space. This approach therefore consisted of 1) creating defining curves for a basis paraboloid (symmetrical or offset) using standard primitives, 2) elongate these with sections of analytical curves describing the blending functions, 3) lofting the adjacent curves together, 4) uniting the multiple surface objects to form a single contiguous surface. A comparison of the reflector surface produced in this way, blue surface, and the reference CAD model as used by the CE based simulation using the formula set out above, yellow surface, can be found presented below in Figure 3b. Here, although the surfaces are in very good agreement, some small differences are evident with, for example, differences in the width of 0.1 mm and the height of ~1 mm. As this larger dimensional difference corresponds to *circa* 1/10th of a wavelength at 26 GHz, this small discrepancy is expected to result in only very minor differences between the respective QZ field simulations.

However, one issue that can persist is the existence of tiny, or very long and thin, triangle mesh cells which are largely created because of the polar form of the surface formulation. Even after a Union Boolean operation, such tiny discontinuities on the edges of the defining curves may not disappear entirely, resulting in very small mesh sizes near the center of the reflector which must be treated manually. The use of Large Element Physical Optics solution usually does not require any further adjustment of the mesh; however, the Physical Optics or Method of Moment solutions almost definitely will require such special attention [11]. Clearly, this has an impact on the simulation precision and solution run-times although a detailed study of this is beyond the scope of this paper and is a planned portion of the future work.

The ~1.1 m BRE reflector CATR was simulated in FEKO using several different solvers however the most encouraging results were obtained when using the Multilevel Fast Multipole Method (MLFMM) [11]. This is an acceleration method that is based on the Method of Moments (MoM) [12] which reduces both the memory requirements and the complexity of the electromagnetic problem. A comparison of the QZ fields can be seen presented in Figure 1 in the form of a false-colour checkerboard plot with the copolar fields being tabulated across a plane transverse to the *z*-axis of the CATR. Here, from inspection, the degree of agreement attained can be seen to be very encouraging. Figure 2 contains comparison plots of the copolar amplitude and phase functions in the vertical axis, which is the dimension in which the two reflector surfaces diverged the most.

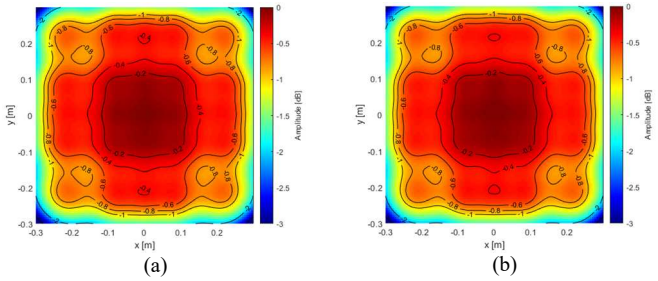

Figure 1: Copolar BRE CATR QZ prediction from (a) FEKO, (b) CE PO Simulation

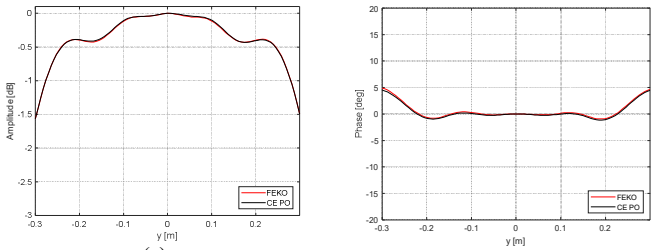

(a) (b)

Figure 2: (a) Comparison of copolar amplitude vertical cuts, and (b) copolar phase vertical cuts of CATR QZ

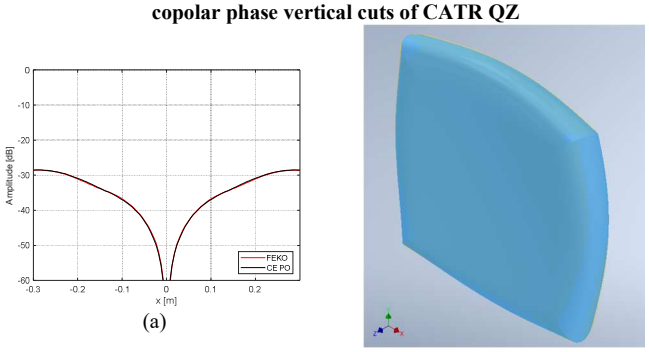

(a) (b)

Figure 3: (a) Comparison of cross-polar amplitude horizontal cuts, and (b) Comparison ~1.1 m BRE CATR Reflector surface, yellow denotes CAD model, blue represents FEKO equivalent

Lastly, Figure 3a contains a cross-polar horizonal cut which again, encouragingly, exhibits a very high degree of agreement despite the very low signal levels involved. Although not shown as a consequence of space constraints; similarly encouraging results were obtained at other frequencies and elsewhere in the QZ. Therefore, when taken together with the previous verification results presented in [10], this can be used to affirm and demonstrate the validity of the extended CE based, parallel, PO CEM model.

C. Genetic Optimization

EM optimization problems generally involve the variation of several parameters. These can be continuous or discrete and are often bounded. These parameters are frequently complex, nonlinear, multiextremal, and nondifferentiable. Genetic Algorithms (GA) are robust, stochastic-based methods which can handle large swathes of EM optimization problems that involve many parameters, and that are not easily accommodated by other techniques, *e.g.* linear parameter sweeps, or a fully random optimization strategy. GAs have therefore been used in many areas of application, including shaped reflector antenna design however their use has largely been restricted to the optimization of field distributions within the Fraunhofer region, rather than the Fresnel region as in this application. The employed genetic optimization algorithm was developed along the general structure presented previously in [6].

```
Begin
   INITIALIZE POPULATION
   REPEAT UNTIL (TERMINATION CONDITION) DO
      EVALUATE NEW CANDIDATES
      PRUNE POPULATION
      CREATE OFFSPRING
   END DO
END
```

Figure 4: Genetic algorithm expressed in pseudocode

An abstracted overview of the used genetic algorithm is presented in Figure 4 with a more general description of the algorithm contained in [13]. The fitness value, *i.e.* penalty function, used was based on an assessment of the ideal QZ field (for antenna measurements) which is the approximation of a plane wave that has constant amplitude and phase in any direction perpendicular to the direction of wave propagation. The fitness value was then computed from the sum of both the standard deviation of the amplitude and the standard deviation of the phase function. It was found that this "summed" normalized fitness value placed equal significance on the uniformity of the amplitude and phase functions. The fitness value is used within the pruning of the population, parent selection and as a termination condition. In case of the termination condition the variation of the fitness value output between iterations is also assessed. As a result of the fitness value strategy optimizing towards an approximation of a plane-wave, ripples are generally minimized inside the QZ in case they have a negative contribution to the plane wave approximation. Therefore, the assessment of the QZ in terms of the separation of taper value using a second order fit and residual ripple [2] does not always show an improvement here, however the improvement in field distribution is clearly shown by visual inspection of the optimized QZ fields.

IV. Simulation Results

To illustrate the effectiveness of the CATR optimization algorithm, an existing CATR designed for 5GNR applications was chosen as a starting point. The mm-wave CATR comprised a floor offset fed reflector that was conceived to provide a 450 mm diameter, cylindrically shaped QZ, with its main operational frequencies residing in the 5G FR2 mm-wave band [1]. The genetic algorithm as described in section III-C above was utilized to simultaneously optimize the boundary, blending and roll parameters r_e, x_m, γ_m, a_e, b_e. The blend function was chosen to follow a cosine-squared function. After selection of the blend functions, the resulting reflector is checked to fit within a predefined maximum outline using an iterative procedure, *cf.* the aforementioned comments in Section IIB regarding the exterior size of the reflector. In this particular case the maximum dimensional envelope was limited to just smaller than ~1.1 x 1.1 meters. The optimization was carried out at 18 GHz, after which the CATRs were simulated at multiple frequencies to ascertain the improvements were not asymptotic and that a broadband solution had been obtained. This is expected as a consequence of the geometrical optics principle upon which the CATR works. The genetic optimization required 25 generations involving ~ 5000 individual simulations and took just a few hours to complete using a typical office laptop, which is very feasible in an industrial setting. The GO was repeated at other frequencies with only very subtlety different evolutions being obtained. In all cases, the curved exterior, *cf.* Figure 5b, was obtained which has the benefit of more evenly distributing the field in the CATR QZ and producing a more even illumination of the interior of the anechoic chamber.

(a) (b)

Figure 5: (a) Rectangular reflector, (b) Genetic optimized reflector

In Figure 5, both the rectangular design used for the baseline simulations and the resulting reflector following genetic optimization are shown. It is noted here that both reflectors fit within the same maximum dimensional envelope noted above. Figure 6 presents cardinal cuts of the CATR QZ co-polar performance in terms of amplitude pattern of the baseline (a) and optimized (b) performance. From inspection of these plots, it is clear that the amplitude behavior, especially at lower frequencies, is smoother and better behaved than the baseline case demonstrating a great deal of uniformity across the frequency band. It was also noted that the optimized CATR was compliant down to *circa* 6 GHz, whereas the unoptimized range was limited to X-band.

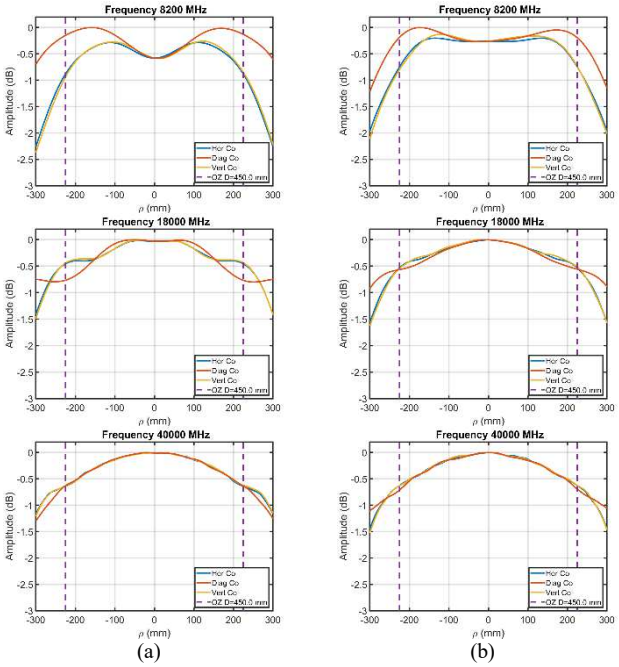

(a) (b)

Figure 6: Co-polar amplitude cuts through the QZ for (a) rectangular shaped, and (b) Genetic-optimized, at 8.2, 18 and 40 GHz

From inspection of Figure 7, it can be seen that the copolar phase distribution is also much smoother down to lower frequencies than was the case for the baseline unoptimized configuration. While also taking the results in Table 1 into account, it was found that even though the reflector was optimized at a single frequency, the frequency response of the range was extremely stable across the very broad band of simulated frequencies. Similarly, and although not shown due to limitations of available space, the cross-polar pattern was also found to contain fewer ripples and was generally far better behaved following the optimization.

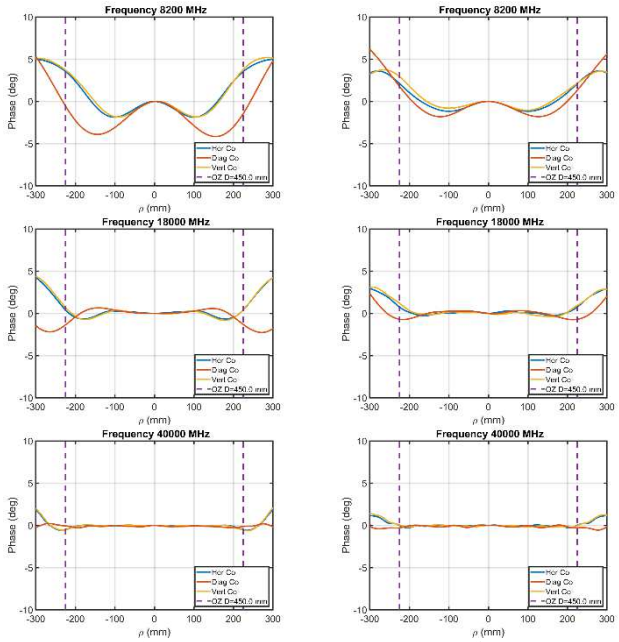

(a) (b)

Figure 7: Co-polar phase cuts through the QZ for (a) rectangular shaped, and (b) Genetic-optimized, at 8.2, 18 and 40 GHz

Table 1 below presents a further assessment of the CATR QZ. Here, F denotes frequency, A_v is amplitude total variation, A_t is amplitude taper [2], A_r is amplitude ripple [2], P_v is phase total variation, [2], and C_p is maximum cross-polar level. All values are worst case for all cuts combined. The cross-polar performance is shown largely for indicative purposes however it was not part of the optimization goal itself as this property is largely governed by the focal length of the parabolic reflector, the feed tilt angle, and the cross-polar performance of the feed, each of which were assumed fixed for the duration of this optimization study.

	Summary of Improvements (+iv-number for all parameters is better except for *Cp* where -iv-number is better)					
***F* [GHz]**	8.2	10	12.4	18	26	40
***A_v* [dB]**	0.0	-0.2	0.1	0.1	0.1	-0.1
***A_t* [dB]**	0.1	-0.3	0.1	0.3	0.0	0.0
***A_r* [dB]**	0.0	0.0	0.1	0.0	0.1	0.0
***P_v* [deg]**	2.3	1.4	0.7	0.6	0.1	0.2
***C_p* [dB]**	-0.2	-0.4	-0.1	-0.7	0.2	0.0

Table 1: Calculated QZ performance for the rectangular & GO design

Based on the examination of all of the results, including those in Table 1, it may be concluded that in practice this particular optimized reflector can be used down to X-band effectively. It is again noted here that both Figure 6 and Figure 7 show very symmetric behavior of the QZ amplitude- and phase-distributions. Therefore, as commented before, it is expected there is little benefit in an individual optimization of the blended rolled edge parameters for each individual φ'angle.

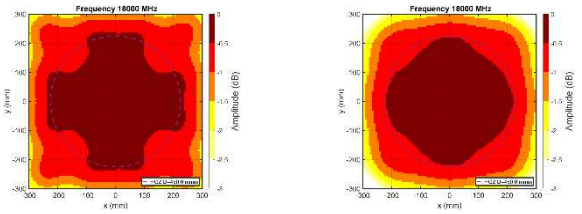

(a) (b)

Figure 8: Co-polar QZ amplitude distribution for (a) rectangular shaped, and (b) Genetic-optimized, at 18 GHz

While reviewing the amplitude distribution through the QZ, as shown in Figure 8, it becomes clear that the optimization of the reflector results in a far more even distribution. It is also noted here that this is the case for all simulated frequencies, however differences, *e.g.* at 40 GHz or higher, become ever smaller.

V. Summary, Conclusion and Future Work

For the first time, this paper has presented the successful application of computational evolution to the design of a BRE CATR using a parallel implementation of an efficient, accurate CE based PO electromagnetic model. Here, the boundary, blending and roll parameters of a blended rolled edge single offset CATR reflector have been optimized using a genetic algorithm. The genetic optimization together with the fast PO-based simulation software allowed a rapid and simultaneous parameter optimization resulting in improvements across all operating frequencies of the range reflector. The presented approach opens new possibilities in tailoring a CATR specifically to a customer's requirements, maximizing the efficiency that chamber space is used while maintaining broad frequency operation. This is important to many customers, however it is of particular relevance to 5G FR2 test applications, especially those involving production test scenarios, where multiple test systems coexist within a single host building. Equally, it is clear that the demonstrated improvements in frequency response allow a broader diversification in the usage of a measurement range, and thus a decrease in total cost of ownership.

The paper has presented the initial work performed within an ongoing study and as such a number of areas for future investigation are still being considered. Among others, replacing the boundary function with a continuous function in φ' will ascertain less discontinuity in surface in the corners of the reflector. One other possible limitation of the current approach is that it is predicated on the assumption that the blended rolled edge provides CATR performance that is inherently broadband in nature, with the optimization process being limited to the examination of a single chosen frequency. However, as this analysis can be readily expanded to operate across a band of frequencies by utilizing the extension of a multi-objective genetic algorithm [13], this is an area that is intended for future investigation. Furthermore, as the optimized CATR performance can be combined with one of the authors pre-existing 5G communications systems performance simulation capability, this optimization technique can be extended to provide facilities that are fully optimized for 5GNR testing.

Acknowledgement

The authors wish to thank Professor Clive Parini for his assistance with the development of the CE PO simulation and to ETS-Lindgren for their support in this work.

References

[1] 3GPP, "TR 37.842 v13.2.0 TSG RAN E-UTRA and UTRA; Radio Frequency (RF) requirement background for Active Antenna System (AAS) Base Station (BS)," 2017.

[2] C. Parini, S. Gregson, J. McCormick, D. Janse van Rensburg and T. Eibert, Theory and Practice of Modern Antenna Range Measurements, 2nd Expanded Edition ed., vol. 1, London: IET Press, 2020.

[3] I. Gupta and W. Burnside, "A Method to Design Blended Rolled Edges for Compact Range Reflectors," The Ohio State University, ElectroScience Laboratory, Columbus, 1989.

[4] T.-H. Lee and W. Burnside, "Compact Range Reflector Edge Treatment Impact on Antenna and Scattering Measurements," *Antennas and Propagation, IEEE Transactions on,* vol. 45, no. 1, pp. 57-65, 1997.

[5] R.-C. Liu and C.-H. Li, "A Novel Design of Compact Antenna Test Range for Ultra-Precise Antenna Test," in *EuCAP*, Dusseldorf, 2021.

[6] M. Dirix and S. F. Gregson, "Optimisation of the Serration Outline Shape of a Single Offset-Fed Compact Antenna Test Range Reflector Using A Genetic Evolution of the Superformula," in *EuCAP*, Düsseldorf, 2021.

[7] C. Pistorius, New Main Reflector, Subreflector and Dual Chamber Concept for Compact Range Applications, Ph.D dissertation, Columbus, Ohio: The Ohio State University, Dept. of Electrical Engineering, 1986.

[8] A. Rudge, K. Milne, A. Olver and P. Knight, The Handbook of Antenna Design Volume I, IEEE Press, 1982.

[9] C. Parini, R. Dubrovka and S. Gregson, "CATR Quiet Zone Modelling and the Prediction of 'Measured' Radiation Pattern Errors: Comparison using a Variety of Electromagnetic Simulation Methods," in *AMTA 37th Annual Meeting & Symposium*, Long Beach California, 2015.

[10] C. Parini, R. Dubrovka and S. Gregson, "Compact Range Quiet Zone Modelling: Quantitative Assesment using a Variety of Electromagnetic Simulation Methods," in *Loughborough Conference on Antennas and Propagation*, Loughborough, 2015.

[11] Altair, *FEKO - EM Simulation Software; Feko info retreived 2016-09-28.*

[12] W. Stutzman and G. Thiele, Antenna Theory and Design, 2nd Edition ed., John Wiley & Sons, inc, 1998.

[13] A. Eiben and J. Smith, Introduction to Evolutionary Computing, Berlin: Springer-Verlag, 2015.